Extreme Mechanics Letters 22 (2018) 112–121

Contents lists available at ScienceDirect

Extreme Mechanics Letters

journal homepage: www.elsevier.com/locate/eml

Buckling and pattern transformation of modified periodic lattice structures

Yuhao He [a,b], Yu Zhou [a], Zishun Liu [a,*], K.M. Liew [b,*]

[a] International Center for Applied Mechanics, State Key Laboratory for Strength and Vibration of Mechanical Structures, Xi'an Jiaotong University, Xi'an, 710049, China

[b] Department of Architecture and Civil Engineering, City University of Hong Kong, Tat Chee Avenue, Kowloon, Hong Kong

HIGHLIGHTS

- The prior buckling mode can be altered by modifying columns in lattice structures.
- There exists an effective modification region which is numerically given out.
- Critical buckling condition of pattern transformation is theoretically analyzed.
- Our findings and methods are validated by numerical and experimental studies.

GRAPHICAL ABSTRACT

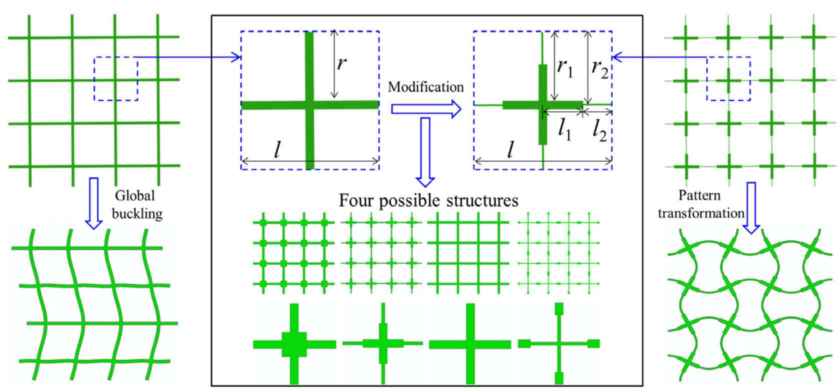

ARTICLE INFO

Article history:
Received 21 April 2018
Received in revised form 30 May 2018
Accepted 31 May 2018
Available online 6 June 2018

Keywords:
Pattern transformation
Periodic lattice structures
Metamaterials
Buckling

ABSTRACT

The prior buckling modes of conventional square lattice structures are always global buckling other than local buckling (i.e., pattern transformation). Interestingly, we found that the preferential buckling mode can be altered to pattern transformation by modifying the sections of the frame in conventional square lattice structures, and there exists an effective modifying region. In order to predict the pattern transformation of this kind of modified structures and to determine the corresponding critical buckling conditions, the theoretical analyses are carried out, and we found that the theoretical results agree well with numerical simulations and experimental studies. This study provides an effective way to achieve pattern transformation based on conventional lattice structures. The presented theoretical approach for predicting critical buckling conditions may shed useful insights on the design and application of lattice metamaterials.

1. Introduction

Metamaterials are engineered multiscale materials whose equivalent physical properties are governed by their architectures rather than compositions. The word "metamaterial" was initially used within the context of optics [1–6] and electromagnetism [7], but today refers to all engineered materials to exhibit novel properties that are not usually found in nature. Mechanical metamaterials have emerged during the last few years partially due to the advances in additive manufacturing techniques that enable the fabrication of complex materials with arbitrary micro-/nano-architectures [8]. As an exciting paradigm, mechanical metamaterials give rise to the developments of materials with unprecedented or rare mechanical properties that could be utilized to

* Corresponding authors.
E-mail addresses: zishunliu@mail.xjtu.edu.cn (Z. Liu), kmliew@cityu.edu.hk (K.M. Liew).

https://doi.org/10.1016/j.eml.2018.05.011
2352-4316/

create advanced materials with novel functionalities [9–11]. These unusual properties include a very high stiffness to weight ratio [12], negative Poisson's ratio [13–16], negative stiffness [17], and negative compressibility under hydrostatic pressure [18]. When artificially and properly designed, mechanical metamaterials can enable acoustic [19] or mechanical [20] cloaking, which are impossible to be observed in conventional materials.

Pattern transformation is a property commonly seen in some mechanical metamaterials when subjected to uniaxial compression beyond a critical value. Many two dimensional or three dimensional metamaterials are designed to achieve this kind of pattern transformation in recent years [21–28]. These mechanical metamaterials include periodic cellular structures [29], regular, chiral and anti-chiral honeycombs [30–32], kirigami geometries [33–35], periodic minimal surface architectures [36] and so on.

Pattern transformation is caused by local elastic instabilities and often reversible and repeatable [29]. Along with this local elastic instability, the periodic lattice metamaterial will undergo a transformation from gradual and homogeneous deformation to a totally different pattern with alternating mutually orthogonal voids. This phenomenon has been observed at macroscales, microscales or even nanoscales [37–39], and many special properties appear with pattern transformation, such as negative Poisson's ratio and new mechanical behaviors. There are many factors affecting pattern transformation including initial porosity [14], arrangement of holes [40,41], loading condition [42–46], shape [21] and inclusions [47,48] of the voids, viscoelastic property [49,50] and combination [22] of the component materials.

Regular honeycombs (or periodic lattice structures) are advanced low-density materials and have widespread application for structural protection, energy absorption and as the core of lightweight sandwich panels [31]. However, the pattern transformation induced by local instability may not be the prior buckling mode of conventional periodic lattice structures. For example, the stress triggers pattern transformation is always higher than that triggers global buckling for square honeycombs [31,51,52], which means that global buckling is the prior buckling mode of conventional square lattice structures. Therefore, if we can realize pattern transformation in conventional lattice structures, it will greatly enlarge the application areas of periodic lattice structures.

Excitingly, we find that the prior buckling mode of conventional square lattice structures can be altered to be pattern transformation by modifying the sections of frames. This study aims at providing an effective way to achieve pattern transformation based on conventional lattice structure and giving out the effective modification region, exploring the mechanical behavior of the modified metamaterials, and proposing a theoretical method to predict the critical buckling conditions for pattern transformation.

The article is organized as follows. First, the geometry of modified lattice metamaterials with stepwise section is presented in Section 2. Then, the numerical and experimental details are introduced in Section 3. Next, the results and discussions are provided in Section 4, including instability analysis results with phase diagrams of first-order buckling modes, theoretical analysis of critical buckling conditions for pattern transformation, the results of numerical and experimental studies, and the discussion about the theoretical prediction and designing method. Finally, the conclusions are presented in Section 5, highlighting the effect of modification (changing the section width at specific position of the frame) on the mechanical response of periodic square lattice structures.

2. Geometries

In this study, we consider a type of modified periodic lattice metamaterials. As shown in Fig. 1, compared with conventional square lattice structures, the modified metamaterials are made by changing the uniform section of frame into stepwise. The structures in blue dash boxes are the primitive cells, which are the minimum constitutional repeating units of periodic structures, for conventional lattice structure (left) and modified lattice structure (right), respectively.

The geometries of modified lattice structures are governed by five parameters, which are the size of a primitive cell, the two widths and the two lengths of the bars with stepwise sections, respectively. The size of the primitive cell is determined by its side length l. The stepwise sections are controlled by r_1 and r_2, which give respective sectional width to be $l - 2r_1$ and $l - 2r_2$. The length of the bars with sectional width of $l - 2r_1$ and $l - 2r_2$ are described by l_1 and l_2, respectively. Since $l_1 + l_2 = l/2$, there are only four independent characteristic parameters.

In present study, the characteristic parameters take the following values. The size of primitive cells is $l = 10$ mm, and the length of the bars with sectional width of $l - 2r_1$ is in the range of 0.1 $\leq l_1/l \leq 0.4$. Noting that there is a natural constraint of $r_1 \geq l_2$ and $r_2 > l_2$, the two sectional width parameters take the value ranges of $l_2/l \leq r_1/l \leq 0.48$ and $0.42 \leq r_2/l \leq 0.48$, respectively. Fig. 2 displays four typical structures that will appear in the modified lattice structures, and the conventional lattice structure ($r_1 = r_2$) is also on the list as shown in Fig. 2(c).

3. Methods

3.1. Numerical simulations

An infinite periodic structure can be modeled by considering a suitable representative volume element (RVE) and applying periodic boundary condition (PBC). The RVE model may consists of one or more primitive cells which depend on the deformation patterns. From previous studies, we know that at least 2 × 2 primitive cells should be employed to characterize the pattern transformation behavior of periodic cellular structures [53]. But the global buckling of periodic cellular structures does not have a periodic cell and the buckled patterns vary as the sizes of the models change. Therefore, the RVE models take 4 × 4 primitive cells considering the difference between pattern transformation and global buckling in this paper.

To determine the effect of column sections on the response of modified periodic lattice structures, numerical simulations are performed with both 2D plane-strain models and 3D solid models using the commercial finite element software ABAQUS. The 8-node biquadratic hybrid plane-strain quadrilateral elements (ABAQUS element type CPE8H) and 8-node linear brick hybrid solid elements (ABAQUS element type C3D8H) are used to generate the mesh of 2D models and 3D models respectively, and the mesh density in 2D models is around 196–1760 elements per primitive cell. The instability analysis is conducted as an eigenvalue problem via the linear buckle analysis by considering RVE models with PBC. Post-buckling analysis is conducted in two manners: (1) considering RVE models with PBC and (2) considering full models. A uniaxial compression of up to 10% nominal strain is applied to investigate the non-linear post-buckling response. The material used in numerical simulation is Tango Black Plus, a type of 3D printing material, and is modeled as nearly incompressible neo-Hookean solid characterized by $K/G = 50$ and $E = 0.53$ MPa.

In the RVE model, two reference points (R_x and R_y) are defined to help apply the boundary conditions. Since the location of reference points makes no difference to the results, R_x and R_y both take the origin of the coordinate. PBC is applied on the parallel opposite edges, which can be expressed as follows with the coordinate system shown in Fig. 2(a),

$$u_{ij} - u_{ij}^{*} = L^{i}\bar{\varepsilon}_{ij} = c_{ij}^{i} \tag{1}$$

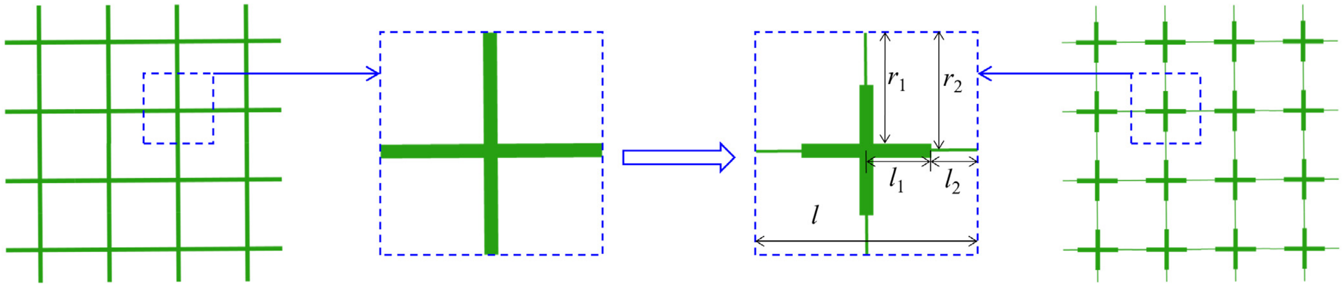

Fig. 1. Schematic of conventional (left) and modified (right) square lattice structures. (For interpretation of the references to color in this figure legend, the reader is referred to the web version of this article.)

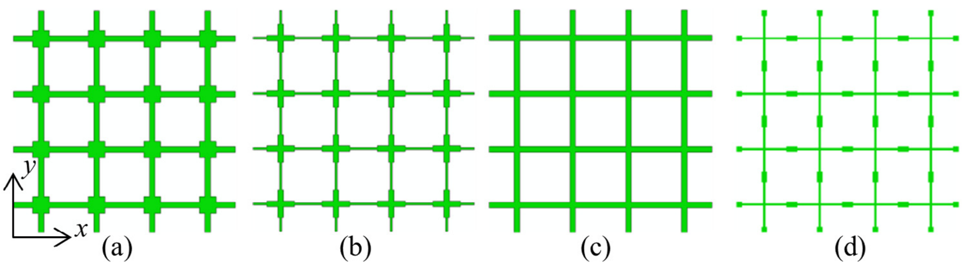

Fig. 2. Typical structures of the modified metamaterials with stepwise sections. (a) $r_1/l = 0.35$, $r_2/l = 0.45$, $l_1/l = 0.15$, (b) $r_1/l = 0.45$, $r_2/l = 0.48$, $l_1/l = 0.25$, (c) $r_1/l = r_2/l = 0.45$, l_1/l for all suitable values, i.e., conventional lattice structures with constant section area, (d) $r_1/l = 0.48$, $r_2/l = 0.45$, $l_1/l = 0.40$.

where u_{ij} and u^*_{ij} are the displacements on the opposite boundary surfaces, L^i and $\bar{\varepsilon}_{ij}$ are the length and average strain of the RVE model, respectively, and c^i_{ij} represents the displacement of the reference point R_i. The indices i and j denote the coordinate directions in the range of x and y. The uniaxial compression load is then applied by giving a displacement c^y_{yy} to R_y in y direction, while the displacement of R_x in x direction is left free. The displacements of R_y in x direction and of R_x in y direction are set to be zero to keep the deformation continuity at the boundaries. To avoid the rigid motion of the model, the center of the left-bottom primitive cell is fixed by setting the displacements in the x and y directions to be zero.

3.2. Experimental details

The modified square lattice metamaterials are fabricated by printing with a multi-material 3D printer (Object350 Connex3, Stratasys Inc., USA). The 3D printing material used is Tango Black Plus, a rubbery material at room temperature, and its Young's modulus is measured to be about 0.53 MPa by quasi-static uniaxial tension test. The performance of our 3D printed lattice structures is tested using quasi-static uniaxial compression, in which the compressive speed of 1 mm/min (i.e., nominal strain rate about 0.00042/s for our samples) is adopted with a Shimadzu testing machine (Shimadzu Corp., Kyoto, Japan), and a camera is used to capture the deformation. The compression process is stopped at a maximum nominal strain of 0.1 after the occurrence of pattern transformation or global buckling. The nominal stress versus nominal strain behavior is recorded and compared with numerical results.

4. Results and discussion

4.1. Instability analysis

Upon application of uniaxial compressive load, a periodic structure can suddenly change its periodicity due to mechanical instability, and such instability can be either microscopic or macroscopic [24]. Here, the instability of the modified square lattice structures is investigated via a linear buckling analysis procedure for all the RVE models mentioned in Section 2. The results of 2D plane-strain models provide us the phase diagram of the first-order buckling mode as shown in Fig. 3. The buckling modes are either pattern transformation (corresponding to solid dots) or global buckling (corresponding to void dots) for different geometric parameter combinations and the pattern transformation region for different l_1/l are filled with different colors. The dots on the blue lines represent the geometric parameter combinations of modified structures similar as shown in Fig. 2(a) (corresponding to the natural constraint $r_1 = l_2$), the dots on the red lines represent the geometric parameter combinations of structures with $r_1 = r_2$ (i.e., the conventional square lattice structures similar as shown in Fig. 2(c). The dots in the regions between the red lines and the blue lines represent the geometric parameter combinations of modified structures similar as shown in Fig. 2(b), and the dots in the regions on the right of the red lines represent the geometric parameter combinations of structures similar as shown in Fig. 2(d).

As we can see from Fig. 3, the pattern transformation only appears in some structures similar to Fig. 2(a) and (b), and the first-order buckling modes are all global buckling modes for structures similar to Fig. 2(c) and (d). The region corresponding to global buckling mode enlarges as the value of l_1/l decreases, and no local buckling mode is observed within our investigation when $l_1/l = 0.15$. So the corresponding distribution of first buckling modes for modified lattice structures with $l_1/l = 0.1$ is not shown in Fig. 3. Besides, the red lines are all located in the global buckling region, which is consistent with the fact that the first-order buckling modes of conventional square lattice structures are global buckling.

It can also be observed that, when $l_1/l > 0.25$, i.e., $l_1 > l_2$, the values of r_1/l and r_2/l have very little effect on the first-order buckling mode; but when $l_1/l < 0.25$, the effect of r_1/l and r_2/l values is quite enormous, and the region corresponding to global buckling mode expands rapidly as l_1/l decreases. On the other hand, no pattern transformation is observed as first-order buckling mode for the modified metamaterials with $l_1/l \leq 0.15$ within our research. It is easy to understand that, when $l_1 \ll l_2$, the modified metamaterials with stepwise sections are very close to conventional square lattice

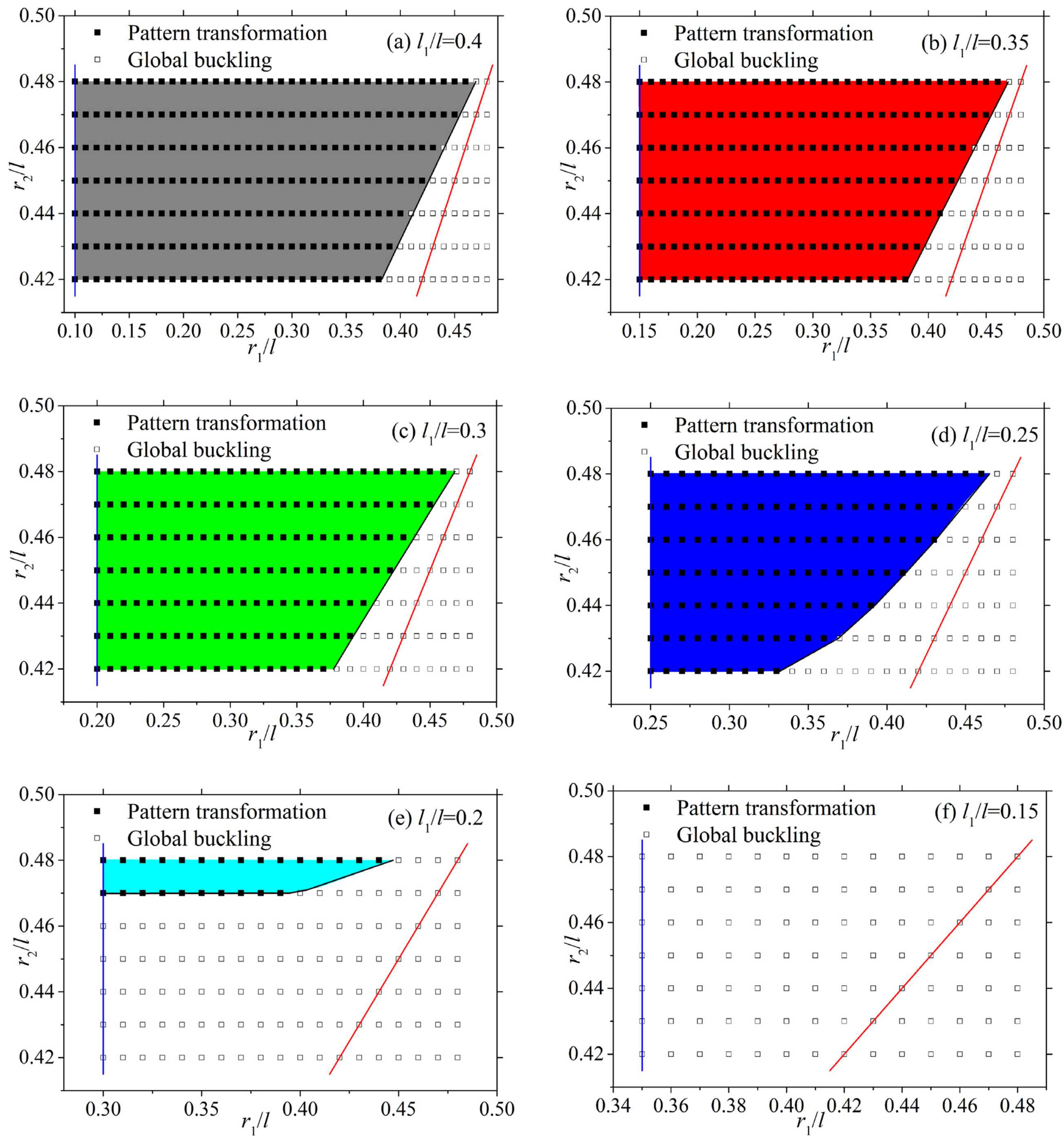

Fig. 3. Phase diagram of the first-order buckling modes for the modified periodic lattice structures with (a) $l_1/l = 0.4$, (b) $l_1/l = 0.35$, (c) $l_1/l = 0.3$, (d) $l_1/l = 0.25$, (e) $l_1/l = 0.2$ and (f) $l_1/l = 0.15$. The colored areas represent the regions of pattern transformation. (For interpretation of the references to color in this figure legend, the reader is referred to the web version of this article.)

metamaterials with a sectional width of $l - 2r_2$. Thus, no matter what the combinations of r_1/l and r_2/l the modified metamaterials are, the first-order buckling modes can only be global buckling. Besides, as the value of r_2/l becomes smaller, the value of r_1/l needed is smaller for pattern transformation as first-order buckling mode, and the smaller the value of l_1/l is, the smaller the value of r_1/l needed. However, note that there is always a region corresponding to pattern transformation as first-order buckling mode when $l_1/l \geq 0.2$, which means that we can achieve pattern transformation by modifying the sections of conventional square lattice structures.

If we set the value of l_1/l as the third axis, superpose all the graphs in Fig. 3 together, and remove most of the data points, we can obtain the graph as shown in Fig. 4. The colored region in Fig. 4 displays the effective combinations of r_1/l, r_2/l and l_1/l corresponding to pattern transformation, while the striped region represents irrational geometric parameter combinations with $r_1 < l_2$ and the rest part corresponds to global buckling. The dash plane represent the geometric parameter combinations of modified metamaterials with $r_1 = r_2$, i.e., the conventional square lattice structures.

Above findings and Fig. 4 can instruct us how to modify the sections of frame to achieve pattern transformation in conventional square lattice structures. Pattern transformation can be realized by slimming down the section at the middle of the columns, but the slimmed area should better not to exceed half length of the

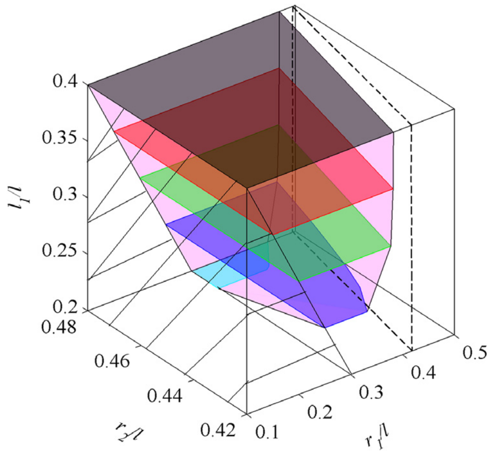

Fig. 4. Effective geometric parameter combinations for modified metamaterials to achieve pattern transformation. (For interpretation of the references to color in this figure legend, the reader is referred to the web version of this article.)

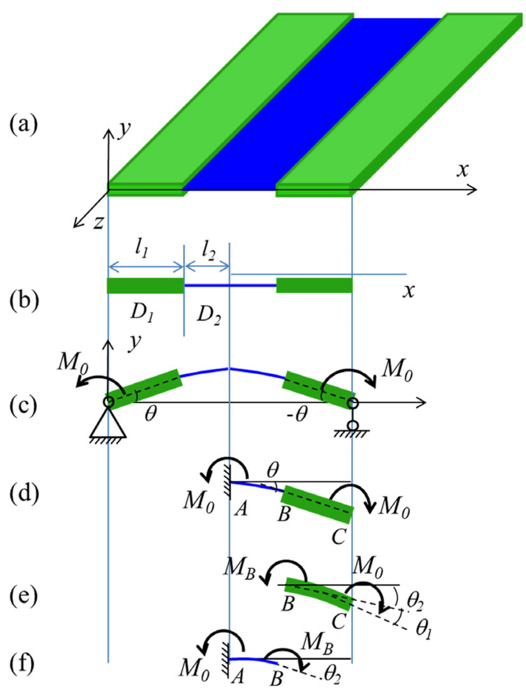

Fig. 5. (a) Oblique view and (b) front view of the plate with stepwise sections. (c) Loading and boundary conditions, (d) Equivalent bending problem, (e) and (f) Free body diagrams of the bending problem.

column, or the effort in achieving pattern transformation will be significantly impaired. Similarly, we can achieve the same goal by widening the sections of the columns at the corners, and the widened area should better exceed half length of the lattice. Besides, as the r_2/l becomes smaller (i.e., the relative section width ($l - 2r_2)/l$ becomes larger), it is more and more difficult to achieve pattern transformation with this method. Since we concern more about pattern transformation, the values of r_2/l taken in this paper are not too small.

4.2. Theoretical analysis

In this section, we focus on the theoretical analysis of pattern transformation. The critical buckling conditions are deduced with the following assumptions. The modified metamaterials are

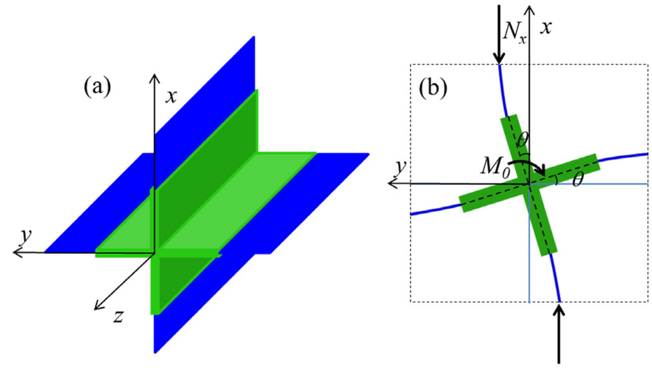

Fig. 6. (a) Oblique view of the initial geometry and (b) front view of the buckled geometry for a primitive cell of modified lattice metamaterial.

assumed to be consisting of plates with stepwise sections and plane-strain deformation problem is considered. Since the buckling occurs at a rather small strain and we are not analyzing the post-buckling behavior, linear buckling is considered. The composition of the material is assumed to be linear elastic.

For a plate with stepwise sections in x-direction and infinite length in z-direction as shown in Fig. 5(a), Fig. 5(b) shows the front view along z-direction. If the plate is simply supported along two opposite edges and subjected by two equal and opposite couples at both hinge joints, the plate will bend as shown in Fig. 5(c). From the symmetric bending shape, we can see that the rotation angle at the middle point of the span is zero and the tangent line of the deflection at this point is horizontal. Thus, the half span of the plate AC can be treated as a cantilever slab as shown in Fig. 5(d). The rotation angle at the free end is equal to the rotation angle θ at the joints, and the relationship between bending moment M_0 and rotation angle θ can be deduced by the method of sections. The free body diagrams of Fig. 5(d) are shown in Fig. 5(e) and (f).

According to the equilibrium equations of segment BC and AB, the internal moment at B is $M_B = M_0$, and then the rotation angles can be obtained to be $\theta_1 = M_0 l_1/D_1$ and $\theta_2 = M_0 l_2/D_2$, where D_1 and D_2 are the bending stiffness and l_1 and l_2 are the lengths of the two cantilever slabs, respectively. Thus, the rotation angle θ at the joints of the simply supported plate can be obtained by summing the rotation angles θ_1 and θ_2 as follows,

$$\theta = \theta_1 + \theta_2 = M_0 \left(\frac{l_1}{D_1} + \frac{l_2}{D_2} \right). \tag{2}$$

The bending stiffness can be expressed as

$$D_1 = \frac{E{w_1}^3}{12\left(1-\nu^2\right)}, \qquad D_2 = \frac{E{w_2}^3}{12\left(1-\nu^2\right)} \tag{3}$$

where E and ν are the Young's modulus and Poisson's ratio of the plates, and w_1 and w_2 are the sectional widths (i.e., the thicknesses of the plates).

As shown in Fig. 6(a), the modified lattice metamaterial with stepwise sections is symmetrical with respect to xz-plane and yz-plane, and each member of the framework with rigid joints can be treated as a plate with elastically restrained ends. The vertical members of the frames are compressed by a normal force N_x, and it is assumed that lateral movement of the joints is prevented by external constraints. When the normal force N_x reaches a critical value, the vertical plates begin to buckle as indicated in Fig. 6(b). This buckling is accompanied by the bending of horizontal plates, and this bending will exert reactive moments to vertical plates at the joints. Hence, the vertical members can be treated as plates with elastically built-in ends.

The moment of vertical plates can be expressed by the following equilibrium differential equations,

$$\begin{cases} D_1 \dfrac{\partial^2 y_1}{\partial x^2} = -N_x y_1 + M_0, & \text{for } 0 \le x \le l_1 \\ D_2 \dfrac{\partial^2 y_2}{\partial x^2} = -N_x y_2 + M_0, & \text{for } l_1 < x \le l/2 \end{cases} \tag{4}$$

where y_i is the deflection and D_i is the bending stiffness of the vertical plates, and the subscript i ($i = 1, 2$) is employed to distinguish the parameters corresponding to different sections. M_0 is the moment exerted by horizontal plates, which can be obtained from Eq. (2). $N_x = F/b$ is the internal normal force in x-direction, and b is the thickness of the modified metamaterial in z-direction.

The general solutions of Eq. (4) are

$$\begin{cases} y_1 = A_1 \sin\alpha_1 x + B_1 \cos\alpha_1 x + \dfrac{M_0}{\alpha_1{}^2 D_1}, & \alpha_1{}^2 = \dfrac{N_x}{D_1} \\ y_2 = A_2 \sin\alpha_2 x + B_2 \cos\alpha_2 x + \dfrac{M_0}{\alpha_2{}^2 D_2}, & \alpha_2{}^2 = \dfrac{N_x}{D_2}. \end{cases} \tag{5}$$

To meet the deformation continuity at $x = l_1$, and consider the boundary conditions at $x = 0$ and $l/2$, the general solutions should satisfy the following equations,

$$\begin{cases} y_1 = y_2, & \dfrac{\partial y_1}{\partial x} = \dfrac{\partial y_2}{\partial x}, & \text{for } x = l_1 \\ y_1 = 0, & \dfrac{\partial y_1}{\partial x} = \theta, & \text{for } x = 0 \\ \dfrac{\partial y_2}{\partial x} = 0, & & \text{for } x = \dfrac{l}{2}. \end{cases} \tag{6}$$

Overall consider above equations, we can deduce the characteristic equation for the critical buckling conditions of pattern transformation as follows,

$$\frac{\alpha_1\left(l_1 + \frac{\alpha_2^2}{\alpha_1^2} l_2\right)\tan\alpha_1 l_1 - 1}{\alpha_1\left(l_1 + \frac{\alpha_2{}^2}{\alpha_1{}^2} l_2\right) + \tan\alpha_1 l_1} \cdot \tan\alpha_2 l_2 = \frac{\alpha_1}{\alpha_2}. \tag{7}$$

With this characteristic equation, considering $N_x = \alpha_1{}^2 D_1 = \alpha_2{}^2 D_2$, the critical buckling force F_{cr} can be obtained with $F_{cr} = \alpha_1^2 D_1 b$ for any given D_1, D_2, l_1, l_2 and b.

Specially, if $D_1 = D_2$, the metamaterial with stepwise section becomes conventional square lattice structures, and we have $\alpha_1 = \alpha_2 = \alpha$ because $F_{cr} = \alpha_1^2 D_1 b = \alpha_2^2 D_2 b$, then Eq. (7) can be simplified to be $\tan(\alpha l/2) + \alpha l/2 = 0$ by considering $l_1 + l_2 = l/2$, which is the same transcendental equation as derived in Ref. [22].

As we all know, the equivalent physical properties of metamaterials are governed by their architectures rather than compositions, therefore it is more meaningful to study the critical buckling strain ε_{cr} rather than the critical buckling force F_{cr}.

For the structure shown in Fig. 6, before the buckling occurs, the deformation is only the compression of the vertical plates, and the stresses for different sections in the vertical plate can be obtained with $\sigma_{1x} = F/(bw_1)$ and $\sigma_{2x} = F/(bw_2)$. For plane-strain problem, the stress and strain follow the following relationship,

$$\varepsilon_x = \frac{1-\nu^2}{E}\sigma_x. \tag{8}$$

The deformations for different sections in the vertical plate can be obtained to be $\Delta l_1 = \varepsilon_{1x} l_1$ and $\Delta l_2 = \varepsilon_{2x} l_2$. Then, we can derive the total strain of the vertical plate to be

$$\varepsilon_x = \frac{\Delta l_1 + \Delta l_2}{l_1 + l_2} = \frac{F(1-\nu^2)}{Eb} \cdot \frac{1}{w_{eq}} \tag{9}$$

where $w_{eq} = (l_1 + l_2)/(l_1/w_1 + l_2/w_2)$ is the equivalent sectional width of modified structures with stepwise sections $w_1 = l - 2r_1$ and $w_2 = l - 2r_2$.

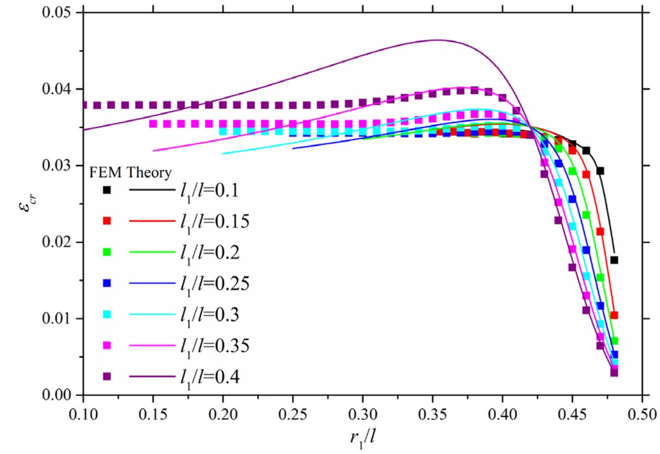

Fig. 7. Critical buckling strain for the pattern transformation of modified metamaterial models with $r_2/l = 0.42$.

Substituting $F_{cr} = \alpha_1^2 D_1 b$ into Eq. (9), we can obtain the critical buckling strain as follows,

$$\varepsilon_{cr} = \frac{1}{12}\frac{\alpha_1{}^2 w_1{}^3}{w_{eq}}. \tag{10}$$

4.3. Comparison between theoretical and numerical results

As discussed above, with different combinations of r_1/l, r_2/l and l_1/l, we can produce various finite element models and calculate out corresponding $\alpha_1{}^2 w_1{}^3$. The critical buckling strains can then be theoretically obtained with Eq. (10) or numerically obtained with finite element analysis. The theoretical results will be compared with the numerical results in the following.

We first focus on a series of modified metamaterials with $l = 10$ mm, $r_2 = 4.2$ mm, $0.1 \le l_1/l \le 0.4$ and r_1 obeying the natural constraint $l_2/l \le r_1/l \le 0.48$. The critical buckling strains for the pattern transformation these modified metamaterials are plotted in Fig. 7. The square dots represent the numerical results and the solid lines represent the theoretical results.

From Fig. 7, we can clearly see that the critical buckling strain decreases as r_1/l increases when r_1/l takes a relatively large value while keeps almost constant when r_1/l takes a relatively small value and the theoretical results only agree well with numerical results when r_1/l takes a relatively large value.

In the same way, for other series of modified metamaterials with $l = 10$ mm, 4.2 mm $\le r_2 \le$ 4.8 mm, $0.1 \le l_1/l \le 0.4$ and $l_2/l \le r_1/l \le 0.48$, the critical buckling strains for pattern transformation can be obtained both by theory and numerical simulation, and the critical buckling strains are presented in Fig. 8. The square dots and solid lines represent the numerical results and theoretical results, respectively.

From Fig. 8, it can be found that, all the critical buckling strains of the modified metamaterials with different r_2/l follow a similar relationship and the theoretical results only agree well with numerical results when r_1/l takes a relatively large value. This is because that the section width $l - 2r_1$ increases as the decrease of r_1/l, and when the section width is large enough, the modified metamaterial cannot be treated as consisting of plates, and thus the formula (10) derived from buckling of plates are not applicable any more. As we can see from Figs. 7 and 8, the critical buckling strains are almost constant for r_1/l <0.3, regardless of the combination of l_1/l and r_2/l. Accordingly, we can learn that the critical buckling strains are the same as long as the slimmed regions are the same, with the same l_1/l and r_2/l, for the conventional lattice structures

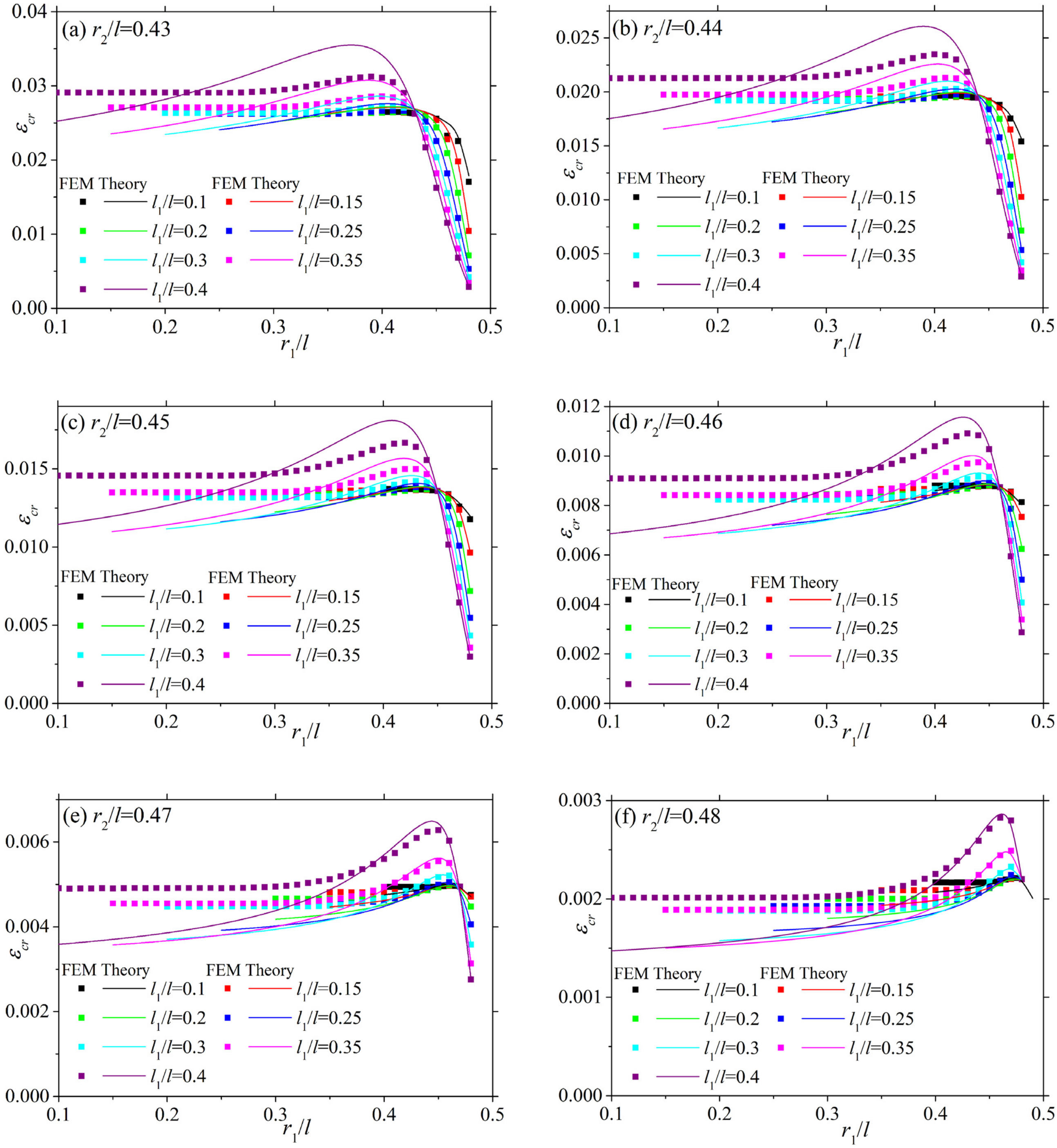

Fig. 8. Critical buckling strain for the pattern transformation of modified metamaterial models with $r_2/l = 0.43$–0.48 (a–f).

with $r/l < 0.3$. Therefore, we can effectively handle the pattern transformation of this kind of structures for desired buckling conditions.

4.4. Effectiveness verification for 3D solid models

From previous analysis, we have known that, pattern transformation can be realized in conventional lattice structures by slimming down the sections in the middle or widening the sections at the corner of the columns, and the slimmed area should better not exceed half-length while the widened area should better exceed half-length of the column. This finding and prediction of buckling strain for pattern transformation have been already proved and validated by the finite element analysis in Sections 4.1 and 4.3 with 2D plane-strain models.

To validate the predictions and formulas for 3D solid models, we have studied three RVE models whose initial sectional shapes are presented in Fig. 9(a). Model I and model III can be treated as slimming down the section in the middle and widening the section at the corners of the columns in model II, respectively. Each models consist of 16 primitive cells with $l_1/l = 0.3$, the size and the thickness of the primitive cell are $l = 10$ mm and $b = 10$ mm, respectively. The compression of the three RVE models are firstly investigated as eigenvalue problem via linear buckle analysis by

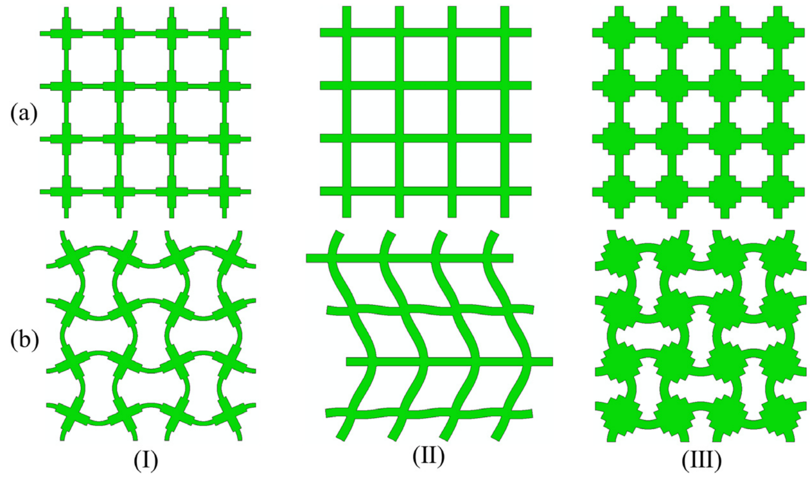

Fig. 9. (a) Initial shapes and (b) first-order buckling patterns of RVE models, (I) $r_1/l = 0.42$, $r_2/l = 0.46$, (II) $r_1/l = r_2/l = 0.42$, (III) $r_1/l = 0.3$, $r_2/l = 0.42$.

Table 1
Critical buckling forces (the value in a single vertical plate) and strains of model I, II and III.

		Model I	Model II		Model III
			Global buckling	Pattern transformation	
Theory	F_{cr} (N)	7.24×10^{-3}	\	0.0392	0.0606
	ε_{cr}	9.08×10^{-3}	\	0.0351	0.0347
RVE model	F_{cr} (N)	5.34×10^{-3}	0.0156	0.0326	0.0432
	ε_{cr}	9.03×10^{-3}	0.0175	0.0356	0.0361
Full model	F_{cr} (N)	4.69×10^{-3}	0.0140	0.0431	0.0375
	ε_{cr}	7.94×10^{-3}	0.0157	0.0289	0.0315

applying PBCs on the parallel opposite edges, and the first-order buckling patterns are shown in Fig. 9(b).

Post-buckling analysis is then conducted in two manners: (1) considering RVE models with PBC and (2) considering full models. As we can see from the buckling patterns in Fig. 9(b), the sections at the top and bottom boundaries of model I and model III are still flat after buckling, but the sections of model II only keep flat in every second horizontal bars. For the compression of full model, the top and bottom sections should better keep flat to eliminate the boundary effects as far as possible. Therefore, the RVE model of model II is altered by another one. Fig. 10(a) and (b) show the post-buckling patterns of the three models in two manners at a nominal strain of 10%. Model II exhibits global buckling while model I and model III exhibit pattern transformation, which proves that by slimming the sections in the middle or widening the sections at the corner of the bars in conventional lattice structures can realize pattern transformation.

Fig. 10(c) and (d) display the experimental images before compression and after compression to a nominal strain of 10%. Compared with the post-buckling patterns obtain from numerical simulations, we can find that the experimental images are slightly different. This is because there are too many uncertain factors during experiments and the boundary conditions during numerical simulations can hardly be consistent with experiments. For example, the friction coefficients of top and bottom surfaces between the sample and the platform, the imperfection of the printed sample, and so on. However, the experimental results are coincident with the numerical results for the prediction that pattern transformation can be realized in conventional lattice structures by slimming down the sections in the middle or widening the sections at the corner of the columns.

As we know that initial geometric imperfection may influence the post-buckling of periodic cellular structures, if we introduce a large enough initial geometric imperfection corresponding to pattern transformation mode, we can also realize pattern transformation in model II. To validate the theoretical prediction of critical buckling force and strain for pattern transformation, we also carry out numerical simulations for model II after introducing into a large enough initial geometric imperfection corresponding to pattern transformation mode. The numerical results for the nominal stress versus nominal strain behavior of the three models, up to a compressive strain of 0.1, are shown in Fig. 11. The behaviors are all characterized by initial linear elastic behaviors with a sudden change to plateau stress. Besides, the departures from linearity for all full models are earlier than that for RVE models, this is because that the application of PBC restricts the deformation at the boundary and makes it difficult for RVE models to alter patterns.

The critical buckling strains and critical buckling force for the three models obtained from numerical results are then compared with theoretical predictions as shown in Table 1.

From the data in Table 1, assuming the numerical results are accurate, we can figure out the relative errors of critical buckling strain between the theoretical predictions and RVE numerical results for model I, model II and model III to be 0.55%, 1.40% and 3.88%, respectively. The discrepancies between theoretical values and numerical results of critical buckling force are caused by the plane-strain conditions considered in the theoretical analysis. If we multiply the theoretical values of critical buckling force by $(1-\nu^2)$, the relative errors of critical buckling force between the theoretical predictions and RVE numerical results for model I, model II and model III can be obtained as 3.03%, 8.63% and 6.60%, respectively.

5. Conclusions

It is well known that global buckling is the prior buckling mode for conventional square lattice structures. But during our study, we find that the preferential buckling pattern can be altered to be pattern transformation by slimming down the sections in

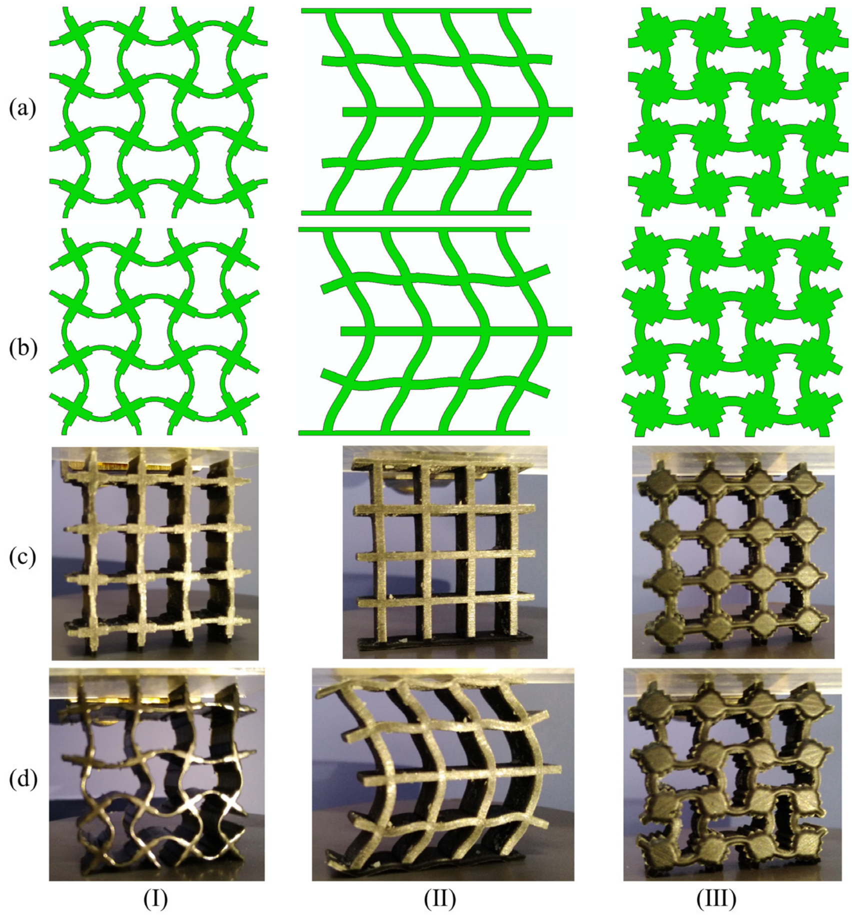

Fig. 10. Post-buckling patterns of three models in two manners: (a) RVE models with PBC and (b) full models at a nominal strain of 10%, and experimental images at a nominal strain of (c) 0 and (d) 10%.

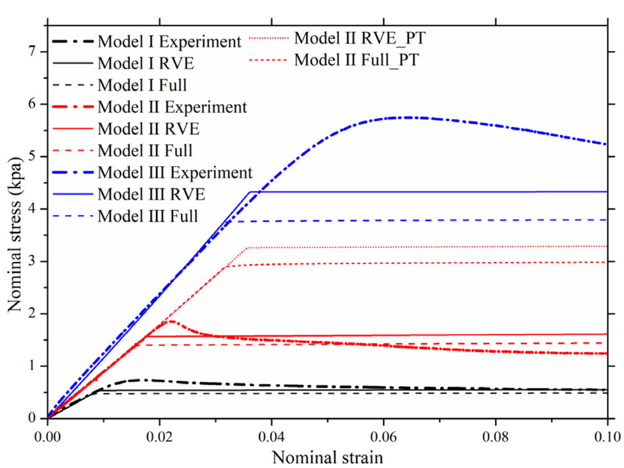

Fig. 11. Nominal stress vs. nominal strain curves for three models showing numerical results (RVE model and full model) and experimental results.

the middle or widening the sections at the corner of the frames in conventional square lattice structures. To prove this, we have studied the buckling behavior for a type of periodic metamaterials constituted by frames with stepwise sections governed by three parameters, l_1/l, r_1/l and r_2/l. With the help of a linear buckling analysis procedure, the phase diagram of first-order buckling modes gives out the effective modifying area. The slimmed area should better not exceed while the widened area should better exceed half-length of the frames, or the effort in achieving pattern transformation will be significantly impaired. Besides, as the relative section width, $(l - 2\,r_2)/l$, becomes larger, it is more and more difficult to achieve pattern transformation with this designing method. Furthermore, we have theoretically analyzed the critical buckling force and critical buckling strain for the pattern transformation of this type of metamaterials. The designing method and theoretical prediction of the critical buckling conditions are verified by numerical simulations and experimental studies. This study provides a possibility to achieve pattern transformation based on conventional lattice structures and a theoretical approach to predict the critical buckling conditions for pattern transformation. We expect our study will contribute to the design and application of lattice metamaterials.

Acknowledgments

The authors are grateful for the support from the National Natural Science Foundation of China through grant numbers: 11572236 and 11372236.

References

[1] B.A. Slovick, Negative refractive index induced by percolation in disordered metamaterials, Phys. Rev. B 95 (9) (2017) 094202.
[2] D.R. Smith, J.B. Pendry, M.C.K. Wiltshire, Metamaterials and negative refractive index, Science 305 (5685) (2004) 788–792.
[3] Z. Li, M. Mutlu, E. Ozbay, Chiral metamaterials: From optical activity and negative refractive index to asymmetric transmission, J. Opt. 15 (2) (2013) 023001.

[4] J. Valentine, S. Zhang, T. Zentgraf, E. Ulin-Avila, D.A. Genov, G. Bartal, X. Zhang, Three-dimensional optical metamaterial with a negative refractive index, Nature 455 (7211) (2008) 376–379.
[5] W. Cai, U.K. Chettiar, A.V. Kildishev, V.M. Shalaev, Optical cloaking with metamaterials, Nat. Photonics 1 (2007) 224.
[6] T. Ergin, N. Stenger, P. Brenner, J.B. Pendry, M. Wegener, Three-dimensional invisibility cloak at optical wavelengths, Science 328 (5976) (2010) 337–339.
[7] C. Caloz, T. Itoh, Electromagnetic Metamaterials: Transmission Line Theory and Microwave Applications, John Wiley & Sons, Hoboken, New Jersey, 2005.
[8] A.A. Zadpoor, Mechanical meta-materials, Mater. Horiz. 3 (5) (2016) 371–381.
[9] J.-H. Lee, J.P. Singer, E.L. Thomas, Micro-/nanostructured mechanical metamaterials, Adv. Mater. 24 (36) (2012) 4782–4810.
[10] C. Coulais, E. Teomy, K. de Reus, Y. Shokef, M. van Hecke, Combinatorial design of textured mechanical metamaterials, Nature 535 (7613) (2016) 529–532.
[11] D. Krishnan, H.T. Johnson, Optical properties of two-dimensional polymer photonic crystals after deformation-induced pattern transformations, J. Mech. Phys. Solids 57 (9) (2009) 1500–1513.
[12] X. Zheng, H. Lee, T.H. Weisgraber, M. Shusteff, J. DeOtte, E.B. Duoss, J.D. Kuntz, M.M. Biener, Q. Ge, J.A. Jackson, S.O. Kucheyev, N.X. Fang, C.M. Spadaccini, Ultralight, ultrastiff mechanical metamaterials, Science 344 (6190) (2014) 1373–1377.
[13] S. Babaee, J. Shim, J.C. Weaver, E.R. Chen, N. Patel, K. Bertoldi, 3d soft metamaterials with negative Poisson's ratio, Adv. Mater. 25 (36) (2013) 5044–5049.
[14] K. Bertoldi, P.M. Reis, S. Willshaw, T. Mullin, Negative Poisson's ratio behavior induced by an elastic instability, Adv. Mater. 22 (3) (2010) 361–366.
[15] N.G. Joseph, C.-G. Roberto, R.D. Mirosław, W.W. Krzysztof, G. Ruben, Smart metamaterials with tunable auxetic and other properties, Smart Mater. Struct. 22 (8) (2013) 084016.
[16] K. Wang, Y.-H. Chang, Y. Chen, C. Zhang, B. Wang, Designable dual-material auxetic metamaterials using three-dimensional printing, Mater. Des. 67 (2015) 159–164.
[17] T. Klatt, M.R. Haberman, A nonlinear negative stiffness metamaterial unit cell and small-on-large multiscale material model, J. Appl. Phys. 114 (3) (2013) 033503.
[18] R.H. Baughman, S. Stafström, C. Cui, S.O. Dantas, Materials with negative compressibilities in one or more dimensions, Science 279 (5356) (1998) 1522–1524.
[19] J. Zhu, T. Chen, Q. Liang, X. Wang, J. Xiong, P. Jiang, A unidirectional acoustic cloak for multilayered background media with homogeneous metamaterials, J. Phys. D: Appl. Phys. 48 (30) (2015) 305502.
[20] T. Bückmann, M. Kadic, R. Schittny, M. Wegener, Mechanical cloak design by direct lattice transformation, Proc. Natl. Acad. Sci. 112 (16) (2015) 4930–4934.
[21] J.Y. Hu, Y.H. He, J.C. Lei, Z.S. Liu, Novel mechanical behavior of periodic structure with the pattern transformation, Theor. Appl. Mech. Lett. 3 (5) (2013) 054007.
[22] Y.H. He, Y. Zhou, Z.S. Liu, K.M. Liew, Pattern transformation of single-material and composite periodic cellular structures, Mater. Des. 132 (2017) 375–384.
[23] K. Bertoldi, Harnessing instabilities to design tunable architected cellular materials, Annu. Rev. Mater. Res. 47 (2017) 51–61.
[24] J. Shim, P. Wang, K. Bertoldi, Harnessing instability-induced pattern transformation to design tunable phononic crystals, Internat. J. Solids Struct. 58 (2015) 52–61.
[25] J.T.B. Overvelde, S. Shan, K. Bertoldi, Compaction through buckling in 2d periodic, soft and porous structures: Effect of pore shape, Adv. Mater. 24 (17) (2012) 2337–2342.
[26] J.T.B. Overvelde, K. Bertoldi, Relating pore shape to the non-linear response of periodic elastomeric structures, J. Mech. Phys. Solids 64 (2014) 351–366.
[27] F. Javid, J. Liu, J. Shim, J. Weaver, A. Shanian, K. Bertoldi, Mechanics of instability-induced pattern transformations in elastomeric porous cylinders, J. Mech. Phys. Solids 96 (2016) 1–17.
[28] X. Ren, J. Shen, P. Tran, T.D. Ngo, Y.M. Xie, Design and characterisation of a tuneable 3d buckling-induced auxetic metamaterial, Mater. Des. 139 (2018) 336–342.
[29] T. Mullin, S. Deschanel, K. Bertoldi, M.C. Boyce, Pattern transformation triggered by deformation, Phys. Rev. Lett. 99 (8) (2007) 084301.
[30] A. Alderson, K.L. Alderson, D. Attard, K.E. Evans, R. Gatt, J.N. Grima, W. Miller, N. Ravirala, C.W. Smith, K. Zied, Elastic constants of 3-, 4-and 6-connected chiral and anti-chiral honeycombs subject to uniaxial in-plane loading, Compos. Sci. Technol. 70 (7) (2010) 1042–1048.
[31] B. Haghpanah, J. Papadopoulos, D. Mousanezhad, H. Nayeb-Hashemi, A. Vaziri, Buckling of regular, chiral and hierarchical honeycombs under a general macroscopic stress state, Proc. R. Soc. Lond. Ser. A Math. Phys. Eng. Sci. 470 (2167) (2014) 20130856.
[32] X.-T. Wang, B. Wang, X.-W. Li, L. Ma, Mechanical properties of 3d re-entrant auxetic cellular structures, Int. J. Mech. Sci. 131 (2017) 396–407.
[33] Y. Tang, J. Yin, Design of cut unit geometry in hierarchical kirigami-based auxetic metamaterials for high stretchability and compressibility, Extreme Mech. Lett. 12 (2017) 77–85.
[34] D. Rayneau-Kirkhope, C. Zhang, L. Theran, M.A. Dias, Analytic analysis of auxetic metamaterials through analogy with rigid link systems, Proc. R. Soc. Lond. Ser. A Math. Phys. Eng. Sci. 474 (2210) (2018) 20170753.
[35] S. Shan, S.H. Kang, Z. Zhao, L. Fang, K. Bertoldi, Design of planar isotropic negative Poisson's ratio structures, Extreme Mech. Lett. 4 (2015) 96–102.
[36] D.W. Abueidda, M. Bakir, R.K. Abu Al-Rub, J.S. Bergström, N.A. Sobh, I. Jasiuk, Mechanical properties of 3d printed polymeric cellular materials with triply periodic minimal surface architectures, Mater. Des. 122 (2017) 255–267.
[37] J.C. Michel, O. Lopez-Pamies, P.P. Castaneda, N. Triantafyllidis, Microscopic and macroscopic instabilities in finitely strained porous elastomers, J. Mech. Phys. Solids 55 (5) (2007) 900–938.
[38] S. Singamaneni, K. Bertoldi, S. Chang, J.H. Jang, S.L. Young, E.L. Thomas, M.C. Boyce, V.V. Tsukruk, Bifurcated mechanical behavior of deformed periodic porous solids, Adv. Funct. Mater. 19 (9) (2009) 1426–1436.
[39] Z.S. Liu, W. Toh, T.Y. Ng, Advances in mechanics of soft materials: A review of large deformation behavior of hydrogels, Int. J. Appl. Mech. 7 (05) (2015) 1530001.
[40] K. Bertoldi, M.C. Boyce, Mechanically triggered transformations of phononic band gaps in periodic elastomeric structures, Phys. Rev. B 77 (5) (2008) 052105.
[41] D. Yang, L. Jin, R.V. Martinez, K. Bertoldi, G.M. Whitesides, Z. Suo, Phase-transforming and switchable metamaterials, Extreme Mech. Lett. 6 (2016) 1–9.
[42] Y. Chen, F. Scarpa, C. Remillat, I. Farrow, Y. Liu, J. Leng, Curved kirigami silicomb cellular structures with zero Poisson's ratio for large deformations and morphing, J. Intell. Mater. Syst. Struct. 25 (6) (2014) 731–743.
[43] K.-L. Chen, Y.-P. Cao, M.-G. Zhang, X.-Q. Feng, Indentation-triggered pattern transformation in hyperelastic soft cellular solids, C.R. Mec. 342 (5) (2014) 292–298.
[44] H. Qiu, Y. Li, T.F. Guo, X. Guo, S. Tang, Deformation and pattern transformation of porous soft solids under biaxial loading: Experiments and simulations, Extreme Mech. Lett. 20 (2018) 81–90.
[45] J. Hu, Y. Zhou, Z. Liu, The friction effect on buckling behavior of cellular structures under axial load, Int. J. Appl. Mech. 0 (0) (2018) 1850013.
[46] C. Coulais, C. Kettenis, M. van Hecke, A characteristic length scale causes anomalous size effects and boundary programmability in mechanical metamaterials, Nat. Phys. 14 (1) (2018) 40–44.
[47] J.Y. Hu, Y.H. He, J.C. Lei, Z.S. Liu, S. Swaddiwudhipong, Mechanical behavior of composite gel periodic structures with the pattern transformation, Struct. Eng. Mech. 50 (5) (2014) 605–616.
[48] T. Mullin, S. Willshaw, F. Box, Pattern switching in soft cellular solids under compression, Soft Matter 9 (20) (2013) 4951–4955.
[49] Y.H. He, S.S. Guo, Z.S. Liu, K.M. Liew, Pattern transformation of thermo-responsive shape memory polymer periodic cellular structures, Internat. J. Solids Struct. 71 (2015) 194–205.
[50] C. Yuan, X. Mu, C.K. Dunn, J. Haidar, T. Wang, H. Jerry Qi, Thermomechanically triggered two-stage pattern switching of 2d lattices for adaptive structures, Adv. Funct. Mater. (2018) 1705727.
[51] N. Ohno, D. Okumura, T. Niikawa, Long-wave buckling of elastic square honeycombs subject to in-plane biaxial compression, Int. J. Mech. Sci. 46 (11) (2004) 1697–1713.
[52] D.J. Rayneau-Kirkhope, M.A. Dias, Recipes for selecting failure modes in 2-d lattices, Extreme Mech. Lett. 9 (2016) 11–20.
[53] K. Bertoldi, M.C. Boyce, S. Deschanel, S.M. Prange, T. Mullin, Mechanics of deformation-triggered pattern transformations and superelastic behavior in periodic elastomeric structures, J. Mech. Phys. Solids 56 (8) (2008) 2642–2668.